

Journal of Structural Geology 21 (1999) 807-819

JOURNAL OF STRUCTURAL GEOLOGY

Constraints on rheology of obsidian lavas based on mesoscopic folds

Jonathan Castro*, Katharine V. Cashman

Department of Geological Sciences, University of Oregon, Eugene, OR 97403, USA

Received 7 September 1998; accepted 16 March 1999

Abstract

The geometry of mesoscopic single and multiple layer folds in rhyolitic obsidian flows is investigated. Folds are composed of obsidian embedded in a matrix of pumice. Folds form by buckling processes as indicated by discontinuous deformation between obsidian and pumice layers and by the geometries of wavetrains. Buckling occurs through a continuum of styles controlled largely by the thickness ratio of pumice to obsidian (N). Styles of folds include chevron, harmonic, polyharmonic, disharmonic and single-layer assemblages. Harmonic and chevron folds are observed for small values of N. For large values of N, folds buckle independently of one another and form disharmonic and single-layer assemblages.

Wavelength-to-thickness ratios of single-layer folds are compared to theoretically predicted ratios for Newtonian and power law fluids as a means of estimating shear viscosity ratios of obsidian and pumice. While all folds indicate that bubble-free rhyolite is more viscous during flow than bubbly rhyolite, estimates of shear viscosity ratio based on Newtonian theory (~10–500), may exceed estimates based on power law rheologies by more than an order of magnitude. Newtonian buckling theory involves a number of simplifications and does not account for the possibly complex rheology of bubble-bearing rhyolite. © 1999 Elsevier Science Ltd. All rights reserved.

1. Introduction

Silicic lava flows provide an opportunity to examine and interpret the deformation behavior of viscous fluids throughout a wide range of flow conditions. Studies of active lava flows and domes allow direct rheological estimates for andesite and dacite lavas (e.g. Anderson and Fink, 1992; Nakada et al., 1995). However the dynamics of rhyolitic obsidian eruptions are difficult to constrain because "no geologist has ever witnessed an obsidian in motion" (Nichols, 1941). Yet rhyolitic activity has dominated the late Holocene volcanic record in many parts of Oregon and California (e.g. Newberry Volcano, South Sister Volcano, Oregon; Medicine Lake Volcano, Mono-Inyo Craters, California). The textural and structural com-

2. Geologic background

Rhyolitic lavas are texturally and structurally heterogeneous. Fink (1983) noted that chemically homogeneous lavas of rhyolitic obsidian flows generally exhibit three textural types: coarsely vesicular pumice (CVP), finely vesicular pumice (FVP), and obsidian (OBS). These lavas differ primarily in their vesicularities and microcrystallinities, and boundaries between types may be sharp or gradational. CVP has numerous (>50%) large vesicles (diameter>1 mm), while FVP

E-mail address: jcastro@darkwing.uoregon.edu (J. Castro)

0191-8141/99/\$ - see front matter \odot 1999 Elsevier Science Ltd. All rights reserved. PII: S0191-8141(99)00070-X

plexities of these Holocene flows are well preserved, and consequently they serve as nearly pristine records of magmatic flow and deformation. The purpose of this work is to describe the deformation style and mechanisms of centimeter- to meter-scale buckle folds in obsidian lavas, and to attempt to constrain the relative rheologic properties of the lavas in which they are formed.

^{*} Corresponding author. Tel.: +541-346-4859; fax: +541-346-4692

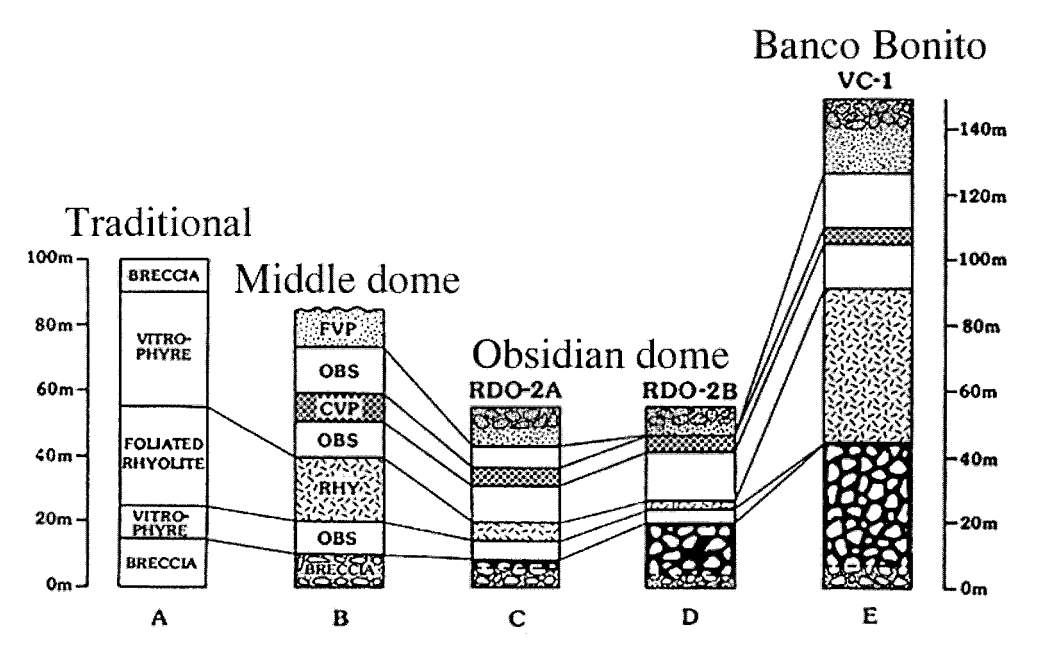


Fig. 1. Cross-sections through four rhyolite flows. (A) 'Traditional' view of rhyolite flows. (B–E): Textural lava types and zonation as revealed by research drilling. FVP=finely vesicular pumice; OBS=obsidian; CVP=coarsely vesicular pumice; RHY=lithoidal rhyolite. Diagonal lines between columns show correlation of textural zones among various flows. Modified from Manley and Fink (1987).

has both lower vesicularity (<40%) and smaller vesicles (diameter <1 mm). Obsidian is, by definition, vesicle poor. The three lava types have consistent contact relations throughout flows and occur in a characteristic stratigraphic order (Fig. 1).

Two contrasting models have been proposed to explain obsidian flow emplacement. The first calls on lava extrusion following explosive activity from a strongly magma chamber zoned in volatiles (Eichelberger and Westrich, 1981; Fink, 1983). According to this model, volatile-rich magma concentrated in the roof of a magma chamber causes initial explosive activity. As the eruption continues, the volatile-rich magma is depleted, and the eruptive style changes to quiescent effusion of extensively degassed magma. In this scenario, the textural complexity of flows (i.e. pumiceous zones and apparent textural stratigraphy; Fig. 1) develops in response to surface vesiculation and post-emplacement redistribution of volatiles (e.g. Fink and Manley, 1987; Fink et al., 1992). An alternative model (e.g. Eichelberger et al., 1986) proposes that obsidian domes form from eruption of highly inflated and gas-charged magma that undergoes collapse during flow advance to form dense black obsidian. According to this model, the magma reservoir has a homogeneous pre-eruption water content, and the eruptive style is dictated by the rate of upward migration of volatiles through a highly inflated and permeable magmatic foam. The erupted magma is

vesicular at the vent, and subsequently collapses under its own weight during flow. In this model, pumiceous zones within obsidian flows are remnant zones of vesiculated lava that did not collapse during flow advance. This permeable foam model requires internal shearing to form obsidian, although structures recording such shear have not been identified.

While models describing the formation of obsidian flows address the development of pumiceous zones and the distribution of volatiles throughout flows, they do not address rheologic variations expected from heterogeneous distributions of bubbles and crystals in the lava. The rheology of rhyolitic magma has been described experimentally as a function of crystal content, water content, melt composition, and temperature (e.g. Shaw, 1972; Murase and McBirney, 1973; Spera et al., 1988). Recently, workers have considered the effects of bubbles on shear viscosity. While Stein and Spera (1992) suggested that bubbles will increase the effective viscosity of the melt, other studies indicate that the addition of bubbles to melt may actually cause a decrease in shear viscosity (Bagdassarov and Dingwell, 1992; Manga et al., 1998). Despite contrasting experimental and theoretical results, it is commonly assumed that bubbles will greatly increase viscosity of the melt, a view that has significant implications for models of magma ascent and vesiculation in volcanic conduits (e.g. Jaupart and Allegre, 1991; Dobran, 1992). Here we provide new constraints on





Fig. 2. (a) Upright and (b) recumbent folds in interlayered obsidian and coarsely vesicular pumice at Big Glass Mountain, California.

the rheology of bubble-bearing rhyolitic melts based on observations and measurements of mesoscopic structures in obsidian flows.

3. Mesoscale deformation in obsidian flows

Deformation of rhyolitic lavas occurs on many scales and is well preserved in Holocene flows. Large-scale (tens of meters) folding forms both recumbent folds and evenly spaced ridges and valleys on flow surfaces (Fig. 2). The geometric relations of these folds have been used to infer flow properties such as viscosity and shear mechanisms (e.g. Fink, 1980, 1984; Smith and Houston, 1994). Microscopic flow dynamics have been investigated by measuring microlite (crystals < 30 μm size) orientation distributions (Manga, 1998). Mesoscopic structures such as buckle folds and boudinage, although very common throughout the flows, have not been studied in detail (Fig. 3).

3.1. Flow layering

Mesoscopic folds and boudinage arise as *flow layer-ing* deforms during flow advance. Flow layering is a

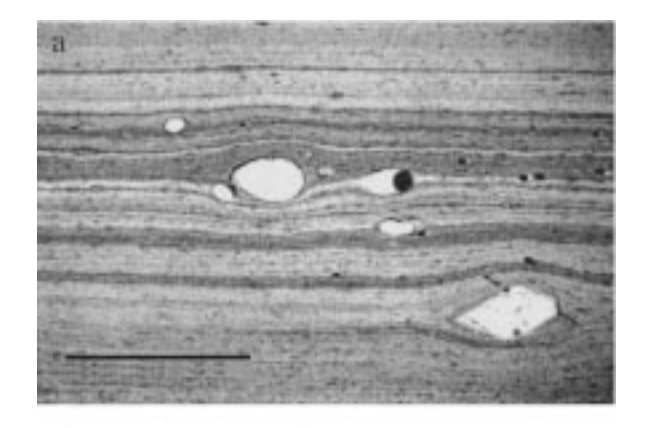


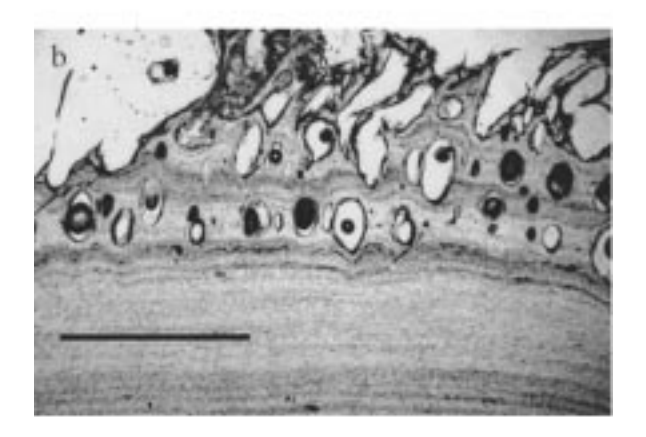
Fig. 3. Oblique view of mesoscopic deformation features in poorly vesicular rhyolite (white bands) and finely vesicular pumice (grey lava) at Panum Dome, eastern California. Hat is 20 cm long.

pervasive structure in obsidian flows (e.g. Manley and Fink, 1987; Swanson et al., 1989). Three types of flow layers exist (Fig. 4). Ubiquitous sub-millimeter scale flow layering is marked by planar variations in microlite concentration. Pumiceous layering consists of planar variations in microlite or vesicle concentration. Textural layering occurs in interlayered obsidian—pumice assemblages and is defined by the alternating arrangement of glassy and pumiceous layers of relatively uniform thickness. Texturally layered lavas are especially well developed at the contacts between obsidian and coarsely vesicular pumice. It is difficult to identify a uniquely primary layering structure because multiple generations of flow layers develop as folds become isoclinal and hinges are transposed.

3.2. Folds

Mesoscopic folds are defined by changes in the shape and orientation of textural flow layers. Single and multilayered folds consist of glassy rhyolite embedded in a matrix of pumice (Fig. 5). Folded layers are always less vesicular than the pumiceous medium in which they are buckled. Rheological differ-





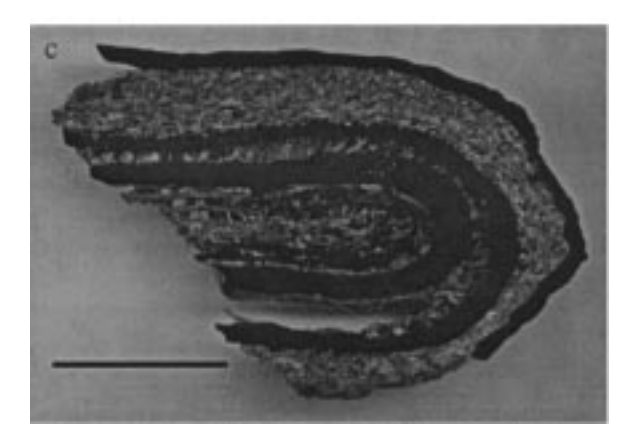


Fig. 4. Three types of flow layering in obsidian lavas. (a) *Microlite defined* flow layers (scale bar = 1 mm). Microlites are approximately 30 μ m in length. Note disruption of microlite flow layering due to formation of large vesicle. (b) *Pumiceous layering* in coarsely vesicular pumice defined by planar layers of vesicles (scale bar = 3 mm). (c) Isoclinally-folded *textural layering* consisting of alternating obsidian (black) and vesicular layers (light grey). Scale bar is 8 cm long.

ences must exist between pumice and obsidian for folds to form. Since major-element compositions of the three textural lava types are uniform within individual flows (Fink, 1982), and crystallinities of fold and matrix vary by only a few volume percent, rheological differences must arise because of variations in microlite

and/or bubble content. Manga (1998) showed that the small volume fraction of microlites in obsidian (~0.01) has a negligible effect on flow viscosity. For this reason, it appears that bubbles exert an important influence on the effective viscosity of silicic lavas and are responsible for rheological variations that lead to the development of folds.

3.3. Boudinage

Boudinage and pinch-and-swell structures are common in layered silicic lavas (Fig. 6). Boudinage, in contrast to folds, forms in response to layer parallel extension. As is the case for folded layers, boudinaged layers are always less vesicular than the pumiceous medium in which they are deformed. Fig. 6 shows an example of boudinage from Panum dome, California. In this structure, a dense glassy rhyolite layer, enveloped in finely vesicular pumice ($\phi \approx 40\%$), underwent layer-parallel extension, and fractured as a result of extreme stretching. It appears that finely vesicular lava subsequently flowed into the void. Subtle necking of the boudinaged layer is recognized as evidence of pinch-and-swell prior to fracture. Given that crystallinities do not vary significantly between the boudinaged and matrix lava, the manner of deformation, and hence, rheologic variations, appear again to be primarily a function of vesicularity differences.

4. Buckle folding

In this section we describe two types of small-scale folds in obsidian flows, single-layer and multilayer buckle folds, and we discuss mechanisms for their formation. Next, we analyze single-layer folds using Newtonian and power-law buckling theories (e.g. Biot, 1961; Smith, 1979) as a means of estimating the shear viscosity ratio of bubble-poor and bubble-rich rhyolite.

Mesoscopic folds commonly form in contact zones between obsidian and coarse pumice, and as parasitic features on larger antiforms (Fig. 7). All folds form by deflection of one or more planar obsidian layers due to some component of layer-parallel compression. Orientations of fold axes are highly variable on the scale of the entire lava flow, but commonly trend parallel to larger-scale folds. The folds discussed here are minor folds (wavelengths less than 100 m) whose geometries are assumed to develop independently of the influence of gravity (e.g. Johnson and Fletcher, 1994).

Such structures can be further classified as buckle folds. In the process of buckle folding, mechanical layering, an alternating arrangement of strong and weak layers, plays an active role in controlling the stress and strain distribution within the layer (e.g. Groshong, 1975). In obsidian flows, mechanical layers



Fig. 5. Single and multilayered glassy folds in coarse pumice: (a) multilayered harmonic, (b) recumbent single-layer isoclinal, (c) intrafolial buckle fold, and (d) polyharmonic folds. Pumice vesicularity is approximately 50%. All exposures are vertical. Hammer is approximately 25 cm long.

are composed of lavas of different vesicularities, for example obsidian and pumice. Evidence that folded obsidian layers are indeed formed by buckling includes: (1) discontinuous deformation across boundaries between pumiceous lava and folded obsidian layers (Fig. 8), suggesting significant mechanical differences across layer boundaries, and thus ruling out passive folding; (2) single-layer folds are a part of semi-regular wavetrains (Ramberg, 1963); and (3) the repeated nature of buckles, which rules out the possibility that folds developed by a transverse bend mechanism (e.g. Groshong, 1975).

Multilayer folds are composed of obsidian layers separated by coarsely vesicular pumice. The amount of pumiceous material between glassy layers varies from approximately 0.1 to 10 cm. The relative thicknesses of pumice and obsidian (pumice/obsidian = N) governs the style of folding. For small values of N, harmonic folds develop. Harmonically folded layers show a correspondence of wavelength and symmetry in all layers (Fig. 9a). With increasing N, and hence sufficiently large separation between layers, the obsidian layers buckle independently of one another and develop their own characteristic wavelength. Under these conditions,



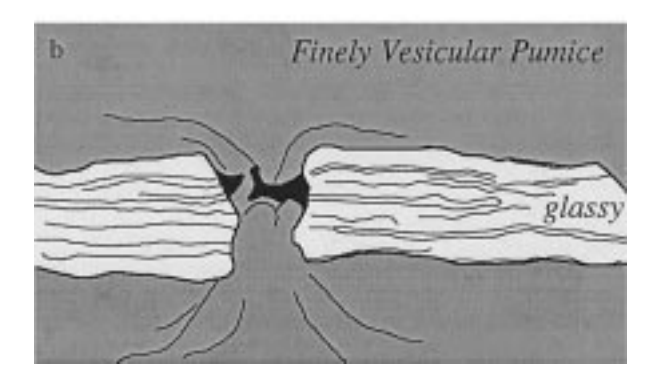


Fig. 6. Boudinage of glassy rhyolite within finely vesicular pumice. (a) Field photograph of vertical exposure of boudinage. (b) Tracing of boudinage. Porosity of boudins is <10% while the porosity of the pumice is approximately 40%. Minor necking of the boudinaged layer in the far right and left portions of the photograph may indicate pinch-and-swell disturbances.

disharmonic and single-layer buckle folds develop (Figs. 9b and c). Fig. 10 shows the average matrix thickness vs average folded-layer thickness for folds from Big Glass Mountain, California. The style of multilayer folds depends on the amount of interlayer pumice, which in turn, implies that lava viscosity is a strong function of bubble content. To address the influence of bubbles on viscosity, we investigate single-layer buckle folds.

Single-layer buckle folds are less common than multilayered fold assemblages, yet occur in the same parts of the flow. Many folds are sinusoidal, and obsidian layers are surrounded by a zone of contact strain in which bubbles are flattened in the fold cores and stretched in the outer arcs of folds (Fig. 11). These folds are typically composed of glassy and poorly vesicular rhyolite 0.1–3 cm thick, buckled within a pumiceous matrix. The vesicularity of the pumice varies from approximately 40 to 85%, with much of the variation attributable to local flattening and extension in and around fold hinges. The overall ptygmatic geometry of these folds suggests large viscosity contrasts between the folded-layer and surrounding matrix (e.g. Ramberg, 1960).





Fig. 7. Parasitic glassy folds in coarse pumice. (a) Vertical exposure of flexural-slip folds on the limb of larger antiform (larger than field of view). (b) Inclined view of an intrafolial buckle fold.

5. Fold analysis

Buckling instabilities arise as a result of contrasts in the strengths of the materials under applied stress (e.g. Smith, 1977). The folds analyzed here are formed during magmatic flow, and hence the rheologic contrasts governing their formation may be viewed as viscosity contrasts. Since structures in obsidian lavas are defined by layered variations in vesicularity, the viscosity contrasts that accompany fold development are most plausibly explained by variations in the bubble content of the melt. Unfortunately there are no direct

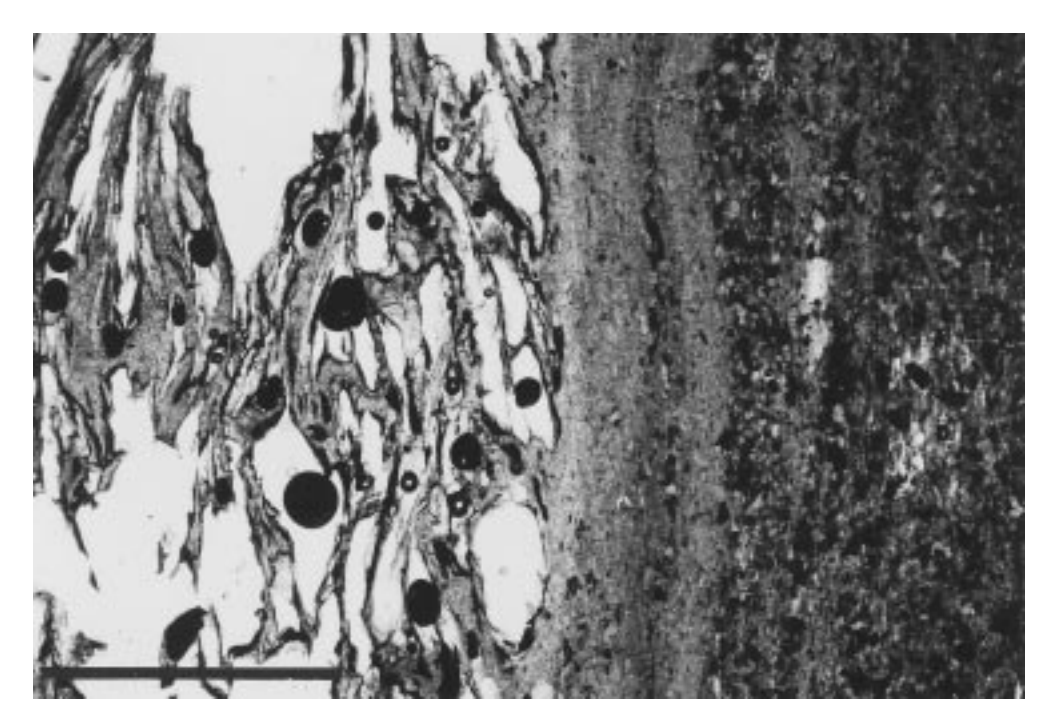


Fig. 8. Photomicrograph of pumice (left) in contact with a folded obsidian layer (right). Strain is localized in the pumiceous lava. Note the deformed vesicles. Scale bar is approximately 3 mm long.

rheological measurements of vesicular rhyolitic lavas. However, geometric relations of folds preserve information regarding the magnitude of the viscosity differences between obsidian and pumice. Below we investigate how wavelength-to-thickness ratios of buckle folds vary, and how such variations may reflect the relative rheologic properties of obsidian and pumice when compared to theoretically predicted wavelength-to-thickness ratios.

5.1. Methods of measurement

In this analysis we seek to relate fold geometry to the relative rheologic and textural characteristics of the fold and matrix. We begin by presenting measurements of four parameters that define the geometry and texture of fold assemblages: arc wavelength (w), layer thickness (T), shortening strain (ε) , and matrix density (ρ) . The arc wavelength is the distance measured perpendicular to fold hinge lines along the center of the folded layer between two successive crests or troughs (Fig. 12). The layer thickness is measured normal to both the folded-layer/matrix interface and the inferred fold axis. Fold wavelength and thickness measurements are used to compute the normalized wavelength (= arc wavelength/thickness) which, in turn, is used to calculate the shear viscosity ratio. Percent shortening was computed by comparing the original length of the folded layer, measured along the centerline of a wave or wavetrain, and the final length of the fold assemblage, measured as the straight-line distance between the ends of fold trains.

The density of the pumiceous matrix is used to calculate porosity (ϕ). Dry bulk density of matrix pumice was determined using Archimedes principle (e.g. Houghton et al., 1988) on samples sawn from fold assemblages. Since pumiceous specimens contain large and irregular vesicles, samples were wrapped in wax film of known volume to prevent infilling of voids with water. Density was determined by weighing wax-coated pumice samples and using the formula:

density
$$(\rho) = \frac{\text{dry wt.}}{\text{dry wt.} - (\text{wax wt.} + \text{wet wt.})}$$

where wax wt. is the wet weight of the wax sheet used to wrap pumice. Matrix densities were determined for 30 samples, each collected from within a 1-5 cm thick envelope around measured fold perimeters. Porosity was determined from the bulk density, assuming a glass density of 2.19 g/cm^3 .

Criteria for fold selection included: (1) assemblages consist of one glassy fold embedded in two-halfspaces of pumice (i.e. no free surfaces); (2) folds exhibit plane strain, as deformation parallel to fold axes appeared to be negligible; (3) folds are not vesicular; (4) folds are symmetrical.

5.2. Folding of Newtonian fluids

Folding theories (e.g. Ramberg, 1960; Biot, 1961) can be used to predict the most stable fold wavelength

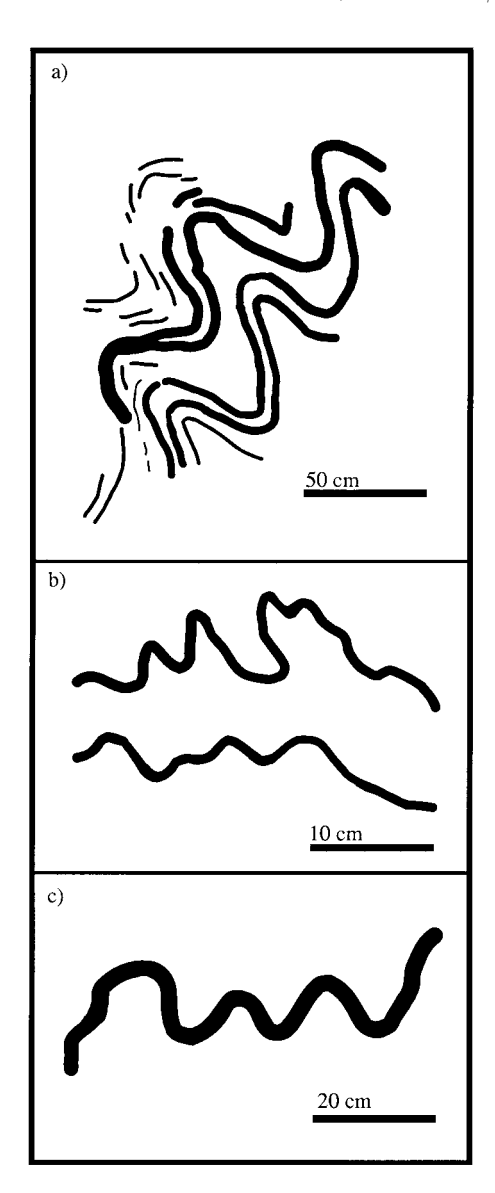


Fig. 9. Tracings of glassy folds ranging from (a) multilayered harmonic, (b) disharmonic, to (c) single-layer ptygmatic. The folding style varies with amount of interlayer pumice and competent layer thickness.

that will grow under conditions of layer-parallel compression and plane strain for a specific shear viscosity ratio and layer thickness. Buckling theory developed by Biot (1961) states that for every fixed layer-matrix shear viscosity ratio, a dominant initial wavelength develops in response to layer-parallel compression. For a Newtonian fluid of shear viscosity $\mu_{\rm II}$ embedded in a medium of shear viscosity $\mu_{\rm II}$, the dominant wavelength of folding ($W_{\rm d}$), layer thickness (T), and shear viscosity ratio ($\mu_{\rm I}/\mu_{\rm II}$) are related by:

$$W_{\rm d} = 2\pi T \left(\frac{\mu_{\rm l}}{6\mu_{\rm m}}\right)^{1/3} \tag{1}$$

(e.g. Ramberg, 1960; Biot, 1961). Note that the domi-

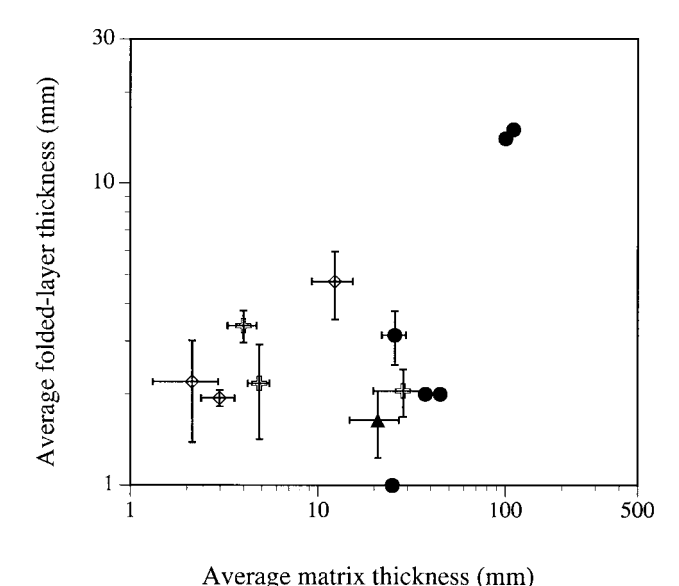


Fig. 10. Phase diagram of multilayered and single-layer folds from Big Glass Mountain. Open symbols represent multilayer harmonic (♦) and polyharmonic (♣) folds. Solid symbols represent disharmonic (♠) and single-layer (•) folds.

nant wavelength is an increasing function of layer thickness and shear viscosity ratio (μ_l/μ_m) . By rearranging Eq. (1), we obtain an expression for the shear viscosity ratio:

$$\frac{\mu_{\rm l}}{\mu_{\rm m}} = 0.024 \left(\frac{w}{T}\right)^3. \tag{2}$$

According to Biot's theory, the arc wavelength (w), as measured through the center of the fold, is assumed to be the dominant initial wavelength that formed at the onset of deformation. However, pre-buckling shortening may lead to modifications of the initial wavelength and therefore introduce error. To address these effects we analyzed the interfaces between foldedlayer and matrix and inspected flow bands internal to the folded layer. Most of the folds analyzed have smoothly curving microlitic flow bands and have nonundulating contacts with the matrix. By contrast, folds that have undergone a finite amount of pre-buckling shortening could be identified by cuspate-lobate interfaces between the matrix and the fold. Only folds not affected by pre-buckling shortening are included in this analysis.

6. Results

Table 1 contains measured and computed parameters for dense glassy folds from Big and Little Glass Mountains, Medicine Lake Volcano, California. Most folds underwent approximately 50% shortening. Because many folds are parts of wavetrains consisting





Fig. 11. (a) Photomicrograph of a single-layer obsidian buckle fold and its pumiceous matrix showing contact strain within the pumice. Scale bar represents 1.5 cm. (b) Close up of deformation in the inner and outer arc regions of the fold. Scale bar represents 0.5 cm.

of several fold arc segments, the values of arc wavelength and layer thickness for each segment are averaged. Although wavelengths and thicknesses vary considerably, average normalized wavelengths vary between 8.0 and 26.4. Matrix vesicularity is also variable (\sim 35–80%), as localized zones of extension and flattening develop in close proximity to a fold (e.g. Fig. 11b).

Arc wavelengths and thicknesses of 73 glassy folds from Big and Little Glass Mountains, and Obsidian Dome, California are presented in Fig. 13. Folds show a general increase in arc wavelength with increasing layer thickness. Wavelength and thickness vary by more than two orders of magnitude. The higher-frequency variation in wavelength observed for folds of constant layer thickness (1–5 cm) is interpreted to be a consequence of changes in the shear viscosity ratio. While this trend is consistent with their for-



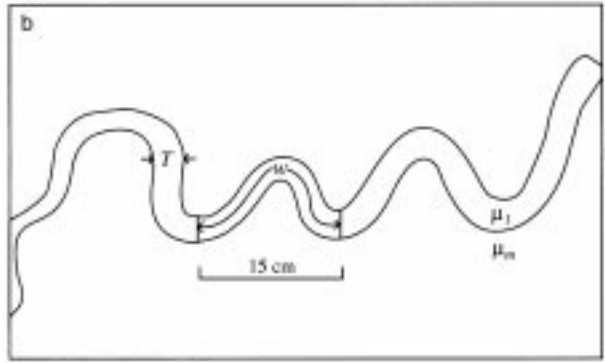


Fig. 12. (a) Vertical exposure of a folded obsidian layer in coarsely vesicular pumice from Big Glass Mountain, California. (b) Trace of the fold showing thickness, T, and are wavelength, w, of the folded layer. $\mu_{\rm l}$ and $\mu_{\rm m}$ are viscosity coefficients of the folded obsidian layer and the pumiceous matrix, respectively. Measurements of wavelength and thickness from this sample indicate that the shear viscosity ratio $(\mu_{\rm l}/\mu_{\rm m})$ is $\cong 33$.

mation by a buckling mechanism (e.g. Ramsay and Huber, 1987), the power law relationship given by Eq. (2) reflects an added influence of the shear viscosity ratio on the dominant wavelength.

Fig. 14 shows the frequency distribution of normalized wavelengths (w/T) for glassy folds from Medicine Lake and Obsidian Dome, California. The preferred normalized wavelength (mode) is approximately 9.5. exhibiting large normalized wavelengths (w/T > 9.5) are interpreted to have buckled under large shear viscosity ratios compared to fold assemblages with smaller normalized wavelengths (w/T < 9.5). Very few folds have wavelengths of less than 6. The preferred normalized wavelength suggests approximately uniform shear viscosity ratios for most of the fold assemblages.

Table 2 shows obsidian-pumiceous rhyolite shear viscosity ratios calculated using Eq. (2). Values are

Table 1
Measured and computed parameters on obsidian folds from Big and Little Glass Mountains, California

Sample*	Thickness (cm) [†]	Wavelength (cm)	Normalized wavelength	% shortening (ε_x)	Matrix porosity
SBG-1	0.46	4.8	10.4	42.2	47.4
SBG-3	1.1	22.1	20.1	55.0	50.0
SBG-40	0.32	5.3	14.3	NA	80.6
SBG-41a	0.44	5.1	11.6	41.0	74.2
SBG-41b	0.11	2.9	26.4	47.0	74.2
SBG-55	0.78	7.6	9.7	51.4	67.0
SBG-59	0.37	4.0	10.8	37.0	NA [‡]
SBG-69	1.3	16.3	12.5	54.0	NA [‡]
BGM-1	0.3	6.1	20.3	8.0	66.0
LGM-9a	1.52	20.0	13.2	60.5	35.5
LGM-9b	4.5	49.0	10.9	32.5	52.2
LGM-11	3.0	39.0	13.0	46.7	65.6
LGM-13	20.0	160	8.0	17.6	51.4

^{*} SBG samples are from distal locations of the southern lobe of Big Glass Mountain while the LGM samples are from the northern perimeter of the north east lobe of Little Glass Mountain.

based on the arc wavelength and folded-layer thickness data presented in Table 1. The estimates indicate that the obsidian shear viscosity (μ_l) may be up to two orders of magnitude greater than pumice shear viscosity (μ_m) . These calculations include two critical assumptions of Newtonian buckling theory: that both media are Newtonian fluids, and the materials maintain constant volume throughout deformation. As these constraints are largely not met in bubble-bearing lava flows, absolute magnitudes of the shear viscosity ratio inferred from normalized wavelengths are not entirely accurate. However, these results indicate that, in contrast to the conventional view of the effect of

bubbles on lava viscosity (e.g. Sibree, 1933; Jaupart and Allegre, 1991), bubbly rhyolitic lava can be less viscous than bubble-poor lava.

7. Discussion

Rheological information is recorded in mesoscopic folds in both their geometries and in the textural differences between folded layers and matrix materials. Newtonian buckling theory (e.g. Biot, 1961) assumes that both materials behave as linear viscous fluids. At low strain rates ($<10^{-3} \, \mathrm{s}^{-1}$) bubble-free rhyolitic melt

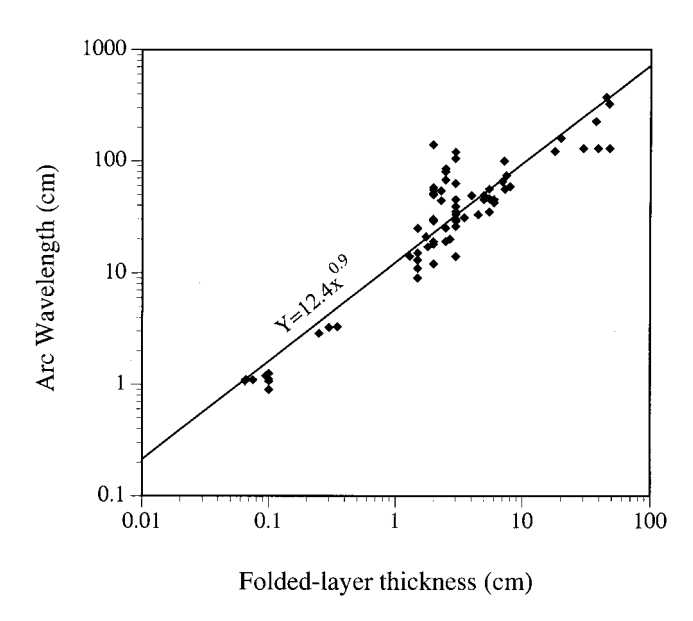


Fig. 13. Plot of arc wavelength vs folded-layer thickness for 73 folds from Big and Little Glass Mountains, California. Curve-fit was determined using the linear least-squares method.

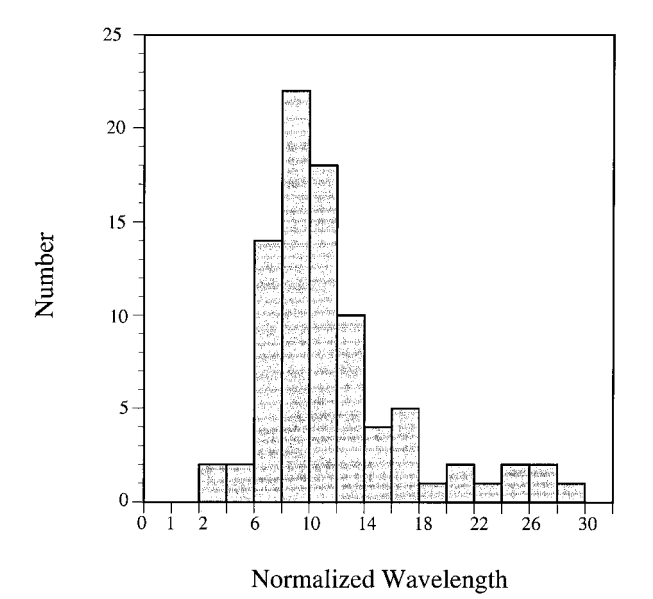


Fig. 14. Distribution of normalized wavelength (w/T) of folds from Big and Little Glass Mountains, and Obsidian Dome, California.

[†] Average layer thickness based on approximately 10 measurements.

[‡] Folding analysis based on photographs.

Table 2
Shear viscosity ratios of folded obsidian layers and pumiceous matrices from Big and Little Glass Mountains, California. Viscosity ratio estimates are based on measured wavelength-to-thickness ratios and theory described by Biot (1961)

Sample*	Shear viscosity ratio (μ_l/μ_m)	Matrix porosity	
SBG-1	28	47.4	
SBG-3	200	50.0	
SBG-40	100	80.6	
SBG-41a	33	74.2	
SBG-41b	500	74.2	
SBG-55	22	67.0	
SBG-59	33	NA^{\dagger}	
SBG-69	50	NA^{\dagger}	
BGM-1	200	66.0	
LGM-9a	50	35.5	
LGM-9b	33	52.2	
LGM-11	50	65.6	
LGM-13	12.5	51.4	

^{*} SBG and BGM samples are from distal locations of the southern lobe of Big Glass Mountain while the LGM samples are from the northern perimeter of the north east lobe of Little Glass Mountain.

may be Newtonian (Webb and Dingwell, 1990). However, bubble-bearing lavas are non-Newtonian (e.g. Stein and Spera, 1992), and suspensions of bubbles may be shear-thinning when bubble deformation is large (Manga et al., 1998). Indeed, pinch-and-swell structures in obsidian flows may be ad-

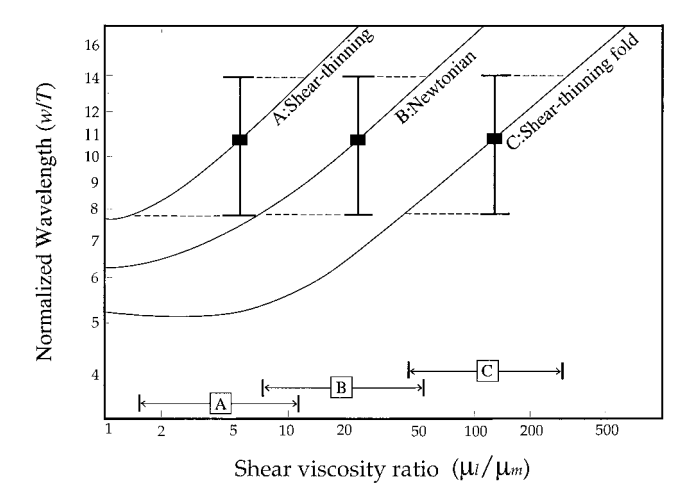


Fig. 15. Normalized wavelength (w/T) plotted against the shear viscosity ratio (μ_l/μ_m) for Newtonian folds buckled in: (A) strongly shear-thinning matrix with power law exponent of 20 and (B) Newtonian matrix. Curve (C) is based on folding of a shear-thinning layer in a shear-thinning matrix whose power law exponents are both 5. For large viscosity ratios the normalized wavelength of folds increases as (μ_l/μ_m)^{1/3} in agreement with classical buckling theory (e.g. Biot, 1961). Error bars represent the standard deviation of average normalized wavelengths of folds from Big Glass Mountain. The upper and lower bounds in normalized wavelength define a range (shown by arrows) in predicted viscosity ratio for the different rheological models. Plot is adapted from Smith (1979).

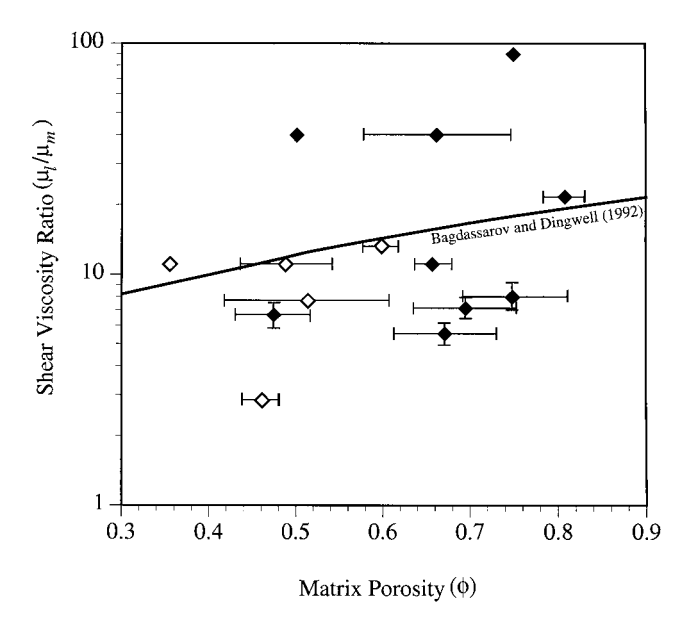


Fig. 16. Relative viscosity vs matrix porosity (vesicularity) for glassy folds from Big Glass Mountain (solid symbols) and Little Glass Mountain (open symbols), California. Error bars represent the standard deviation in average porosity and relative viscosity. Points without error bars represent single wavelength and porosity measurements. Relative viscosities were determined graphically using curve (A) from Fig. 14 and therefore represent estimates based on folding of a Newtonian layer within a strongly shear-thinning matrix. Solid curve represents the best-fit to experimental data of Bagdassarov and Dingwell (1992).

ditional evidence that flow was non-Newtonian (e.g. Smith, 1975, 1977; Emerman and Turcotte, 1984). An obsidian layer buckled in pumice may represent an assemblage in which the folded layer (obsidian) behaves as a Newtonian fluid while the matrix (pumice) behaves as a non-Newtonian fluid. A theoretical framework concerning such a rheologic configuration is presented by Smith (1979).

Fig. 15 shows curves of normalized wavelength vs shear viscosity ratio predicted for fluids with both Newtonian and power law rheologies (Smith, 1977, 1979). The average normalized wavelengths of 17 buckle folds from Big Glass Mountain are shown for: (A) Newtonian folds embedded in a shear-thinning medium, (B) Newtonian fold-matrix pairs, and (C) shear-thinning folds in a shear-thinning matrix. These folds were chosen because they are completely devoid of vesicles (end-member obsidian) and formed under plane strain conditions. Error bars provide the standard deviation of the normalized wavelength, which, in turn, provides a range in shear viscosity ratio according to the various model curves. In the context of Newtonian theory, the variance in normalized wavelength corresponds to a range in shear viscosity ratio of $\sim 7-55$. Comparable Newtonian folds of the observed average normalized wavelength buckled in a shear-thinning matrix would be produced over a range

[†] Folding analysis based on photographs.

in shear viscosity ratio of $\sim 1.5-12$. A shear-thinning fold buckled in a shear-thinning matrix would correspond to a range in shear viscosity ratio of $\sim 45-350$ (e.g. curve C, Fig. 15). At least qualitatively, then, shear-thinning behavior accentuates the viscosity contrast between obsidian and pumice, and leads to the formation of a larger wavelength than would be produced in Newtonian media. If pumiceous rhyolite is shear-thinning, and if obsidian is Newtonian during flow, estimates of shear viscosity ratio based on Biot's theory may be high by more than a factor of 10.

Fig. 16 shows the shear viscosity ratio of glassy fold assemblages from Big and Little Glass Mountains plotted vs matrix vesicularity. Viscosity ratio estimates are based on curve A, Fig. 15. The highly variable matrix vesicularity renders a diffuse correlation between shear viscosity ratio and bubble content. However, the general increase in shear viscosity ratio with increasing matrix porosity is consistent with experimental results (solid line; Fig. 16) from Bagdassarov and Dingwell (1992). While estimates of viscosity ratio based on non-Newtonian rheology do not correspond directly with those found experimentally by Bagdassarov and Dingwell (1992), most of the samples plot within one order of magnitude of their shear viscosity estimates.

Given that no direct measurements of the viscosity of rhyolitic lavas are available, and experimentally determined viscosities of bubbly rhyolitic melts are scarce (Bagdassarov and Dingwell, 1992), testing rheological inferences based on comparisons of measured and theoretically predicted fold wavelengths is difficult to impossible. While we would be overly optimistic to assume that precise values of shear viscosity ratio may be obtained by the applications of Biot (1961) and Smith (1979) folding theories, bubbly rhyolite appears at least qualitatively to be less viscous than bubble-free rhyolite. This result explains the common occurrence of both mesoscopic folds and boudinage in layered silicic lavas.

8. Conclusions

Analysis of intermediate-scale buckle folds yields insights into both the deformation mechanisms and the relative rheologic properties of obsidian lavas. Buckle fold style is determined by the relative spacing of obsidian layers and intervening pumice. This follows from the fact that obsidian layers can translate past one another along planes of less viscous pumiceous lava. Hence, flexural-slip folding appears to be the dominant mode of deformation in shortened, texturally layered lavas. The observation that folded and boudinaged layers are always less vesicular than the surrounding pumiceous matrix is primary evidence

that bubble-poor lava behaves less viscously than bubbly lava. Single-layer buckle folds and boudinage may therefore be used as qualitative indicators of the relative shear viscosities of bubble-poor and bubbly silicic lavas. However, accurately quantifying shear viscosity ratios from the geometries of these structures is not straightforward. Viscosity ratio estimates (~1.5–12; Fig. 15) based on a non-Newtonian model (Smith, 1979) may be more reliable than Newtonian estimates (~10–500; Table 2) if bubble-bearing rhyolitic melts are shear thinning (e.g. Manga et al., 1998).

The rheological evidence offered by mesoscopic structures, while qualitative, is relevant to placing better constraints on the formation and structural evolution of obsidian flows. If obsidian flows are indeed stratified with respect to vesicularity (see Fig. 1), the rheologic properties of the flow must also vary in a compatible manner and therefore, the structural evolution of the flow should be strongly dependent on the location and timing of formation of zones of bubblerich lava. Late-stage vesiculation of obsidian flow interiors (e.g. Fink et al., 1992) may promote rheologic contrasts similar to those inferred from mesoscopic buckle folds. Such large-scale rheologic gradients may be an important influence in the development of structures such as flow ridges (e.g. Fig. 2) and cavity structures (Jensen, 1993).

Acknowledgements

B. Olmstead and N. Joslin assisted in sample collection. M. Manga provided comments. G. Davis, R. Patton, S. Cashman, and A. Watkinson made many valuable suggestions during the preliminary stages of this work. The authors benefitted immensely from comments by J. Dixon, S. Ghosh, and R. Lisle. This work was supported by grants from the Geological Society of America and the Sigma Xi scientific society, and by NSF grant EAR-9614753 to K. Cashman.

References

Anderson, S.W., Fink, J.H., 1992. Crease structures: indicators of emplacement rates and surface stress regimes of lava flows. Geological Society of America Bulletin 104, 615–625.

Bagdassarov, N., Dingwell, D.B., 1992. A rheological investigation of vesicular rhyolite. Journal of Volcanology and Geothermal Research 50, 307–322.

Biot, M.A., 1961. Theory of folding of stratified viscoelastic media and its implication in tectonics and orogenesis. Geological Society of America Bulletin 72, 1595–1620.

Dobran, F., 1992. Nonequilibrium flow in volcanic conduits and application to eruptions of Mt. St. Helens on May 18, 1980, and Vesuvius in AD 79. Journal of Volcanology and Geothermal Research 49, 285–311.

Eichelberger, J.C., Westrich, H.R., 1981. Magmatic volatiles in

- explosive rhyolitic eruptions. Geophysical Research Letters 8, 757–760.
- Eichelberger, J.C., Carrigan, C.R., Westrich, H.R., Price, R.H., 1986. Non-explosive silicic volcanism. Nature 323, 589–602.
- Emerman, S.H., Turcotte, D.L., 1984. A back-of-the-envelope approach to boudinage mechanics. Tectonophysics 110, 333–338.
- Fink, J.H., 1980. Surface folding and viscosity of rhyolite flows. Geology 8, 250–254.
- Fink, J.H., 1982. Surface structure of Little Glass Mountain. In: Johnston, D.A., Donnelly-Nolan, J. (Eds.), Guides to Some Volcanic Terranes in Washington, Idaho, Oregon, and Northern California, 838. United States Geological Survey Circular, pp. 171–176.
- Fink, J.H., 1983. Structure and emplacement of a rhyolitic obsidian flow: Little Glass Mountain, Medicine Lake Highland, northern California. Geological Society of America Bulletin 94, 362–380.
- Fink, J.H., 1984. Structural geologic constraints on the rheology of rhyolitic obsidian. Journal of Non-crystalline Solids 67, 135–146.
- Fink, J.H., Manley, C.R., 1987. Origin of pumiceous and glassy textures in rhyolite flows and domes, Fink, J.H. (Ed.), The Emplacement of Silicic Domes and Lava Flows. Geological Society of America Special Paper 212, pp. 77–89.
- Fink, J.H., Anderson, S.W., Manley, C.R., 1992. Textural constraints on silicic volcanism: beyond the permeable foam model. Journal of Geophysical Research 97, 77–88.
- Groshong, R.H., 1975. Strain, fractures, and pressure solution in natural single-layer folds. Geological Society of America Bulletin 86, 1363–1376.
- Houghton, B.F., Wilson, C.J.N., Hassan, M., 1988. Density measurements for pyroclasts and pyroclastic rocks. New Zealand Geological Survey Record 35, 73–76.
- Jaupart, C., Allegre, C.J., 1991. Gas content, eruption rate and instabilities of eruption regime in silicic volcanoes. Earth and Planetary Science Letters 102, 413–429.
- Jensen, R.A., 1993. Explosion craters and giant gas bubbles on Holocene rhyolite flows at Newberry Crater, Oregon. Oregon Geology 55, 13–19.
- Johnson, A.M., Fletcher, R.C., 1994. Folding of Viscous Layers. Columbia University Press, New York.
- Manga, M., 1998. Orientation distribution of microlites in obsidian. Journal of Volcanology and Geothermal Research 86, 107–115.
- Manga, M., Castro, J.M., Cashman, K.V., Loewenberg, M., 1998. Rheology of bubble-bearing magmas. Journal of Volcanology and Geothermal Research 87, 15–28.
- Manley, C.R., Fink, J.H., 1987. Internal textures of rhyolite flows as revealed by research drilling. Geology 15, 549–552.
- Murase, T., McBirney, A.R., 1973. Properties of some common

- igneous rocks and their melts at high temperatures. Geological Society of America Bulletin 84, 3563–3592.
- Nakada, S., Miyake, Y., Sato, H., Oshima, O., Fujinawa, A., 1995. Endogenous growth of dacite dome at Unzen volcano Japan. Geology 23, 157–160.
- Nichols, R.L., 1941. The velocity of the Big Obsidian Flow, Bend, Oregon. Transactions of the American Geophysical Union, 504– 505.
- Ramberg, H., 1960. Relationship between length of arc and thickness of ptygmatically folded veins. American Journal of Science 258, 36-46.
- Ramberg, H., 1963. Strain distribution and geometry of folds. Uppsala University Geology Institute Bulletin 42, 1–20.
- Ramsay, J.G., Huber, M., 1987. In: The Techniques of Modern Structural Geology, Volume 2: Folds and Fractures. Academic Press, London.
- Shaw, H.R., 1972. Viscosities of magmatic silicate liquids: an empirical method of prediction. American Journal of Science 266, 225–264.
- Sibree, J.O., 1933. The viscosity of froth. Transactions of the Faraday Society 28, 325–331.
- Smith, R.B., 1975. A unified theory of the onset of folding, boudinage, and mullion structure. Geological Society of America Bulletin 86, 1601–1609.
- Smith, R.B., 1977. Formation of folds, boudinage, and mullions in non-Newtonian materials. Geological Society of America Bulletin 88, 312–320.
- Smith, R.B., 1979. The folding of a strongly non-Newtonian layer. American Journal of Science 279, 272–287.
- Smith, J.V., Houston, H.C., 1994. Folds produced by gravity spreading of a banded rhyolite flow. Journal of Volcanology and Geothermal Research 63, 89–94.
- Spera, F.J., Borgia, A., Strimple, J., Feigenson, M.D., 1988. Rheology of melts and magmatic suspensions: Design and calibration of concentric cylinder viscometer with application to rhyolitic magma. Journal of Geophysical Research 93, 10273–10294.
- Stein, D.J., Spera, F.J., 1992. Rheology and microstructure of magmatic emulsions: theory and experiments. Journal of Volcanology and Geothermal Research 49, 157–174.
- Swanson, S.E., Naney, M.T., Westrich, H.R., Eichelberger, J.C., 1989. Crystallization history of Obsidian Dome, Inyo Domes, California. Bulletin of Volcanology 51, 161–176.
- Webb, S.L., Dingwell, D.B., 1990. Non-Newtonian rheology of igneous melts at high stresses and strain rates: Experimental results for rhyolite, andesite, basalt, and nephelinite. Journal of Geophysical Research 95, 15659–15701.